

Avoiding unphysical kinetic traps in Monte Carlo simulations of strongly attractive particles

Stephen Whitelam and Phillip L. Geissler

*Department of Chemistry, University of California at Berkeley,
and Physical Biosciences and Materials Sciences Divisions,
Lawrence Berkeley National Laboratory, Berkeley, CA 94720*

(Dated: February 8, 2020)

We introduce a ‘virtual-move’ Monte Carlo (VMMC) algorithm for systems of pairwise-interacting particles. This algorithm facilitates the simulation of particles possessing attractions of short range and arbitrary strength and geometry, an important realization being self-assembling particles endowed with strong, short-ranged and angularly specific (‘patchy’) attractions. Standard Monte Carlo techniques employ sequential updates of particles and suffer from low acceptance rates when attractions are strong. Our algorithm avoids this slowing-down by proposing simultaneous moves of collections (clusters) of particles. One particle first executes a ‘virtual’ trial move. We determine which of its neighbours move in a similar fashion by calculating individual bond energies before and after the proposed move. We iterate this procedure and update simultaneously the positions of all affected particles. Particles move according to an approximation of realistic dynamics without requiring the explicit computation of forces, and without the step size restrictions required by molecular dynamics simulations. We also employ a size- and shape-dependent hydrodynamic damping of cluster movements. We discuss the virtual-move algorithm in the context of other Monte Carlo cluster-move schemes, and demonstrate its utility by applying it to a model of biological self-assembly.

PACS numbers: 02.70.Tt, 87.53.Wz

I. INTRODUCTION

A standard Monte Carlo simulation of a system of particles consists of a sequence of moves of individual particles. If these moves are proposed and accepted according to the principle of detailed balance (or balance [1, 2] or superdetailed balance [3]), the system will eventually relax to thermal equilibrium [4]. This approach even provides an approximation to the dynamics that the corresponding physical system would execute [5, 6, 7]. However, equilibration can become very slow when relaxation requires the movement of particles in concert, particularly in the presence of very strong interactions. This is the case, for example, when small ions of opposite charge bind together tightly [8].

In Figure 1 we show a simple situation in which a standard Monte Carlo simulation experiences a dramatic slowing-down. We consider four particles, endowed with strong, short-ranged pair interactions, with only two (j and k) close enough to interact. Tightly-bound particles such as j and k are likely to move in concert. Molecular dynamics simulations accomplish this collective movement by updating *simultaneously* the position of every particle: if j or k moves, the force on the other is calculated and the positions of both corrected. A standard Monte Carlo simulation, however, employs *sequential* updates of individual particle positions. Any move (e.g. $\mathbf{a} \rightarrow \mathbf{b}$) of particle j or k which breaks the jk interaction is suppressed by the exponential of the dimer binding energy. If this energy is but a few multiples of $k_B T$, such a break is almost never accepted. In order for the dimer to move substantially, the single-particle move must be

so small that it does not break the short-ranged bond. This leads to very long relaxation times and unphysical mechanisms of evolution.

This problem can be overcome in principle by proposing a simultaneous move of particles j and k ($\mathbf{a} \rightarrow \mathbf{c}$), or in general moves of clusters of particles. Existing cluster algorithms [9, 10, 11, 12, 13] have been used with great success to simulate many complex systems [15]. Such algorithms define a cluster to be moved by recursively linking particle pairs with a given probability. In general, this probability is $p = 1 - e^{\beta \epsilon}$, which depends on the reciprocal of the Boltzmann weight associated with the pair energy $\epsilon < 0$. This choice makes efficient use of computer resources, because detailed balance dictates that moves of clusters defined in this manner are always accepted, provided that no particle overlap occurs.

However, these rejection-free algorithms encounter problems when the attraction strength $-\epsilon$ between particles becomes very large. Strongly-bonded particles are invariably assigned to the same cluster, and so are not moved relative to each other. Thus the possibility of replacing their strong bond with one even stronger is rarely tested. Such unphysical kinetic traps severely impede the relaxation of dense, ordered structures, by preventing the particles comprising a cluster from exploring local gradients in potential energy. These explorations occur in many phase transitions, such as the microphase separation of colloids at low temperature, and in self-assembly, e.g. of large proteins called chaperonins [16, 17, 18]; various nanoparticles [19, 20, 21]; and virus capsids [22, 23].

In this paper we first show that one can avoid the unphysical traps plaguing conventional cluster moves in a computationally efficient way. Particle pairs are linked

with a probability depending on a pseudo-Boltzmann weight containing a fictitious temperature T_f in general greater than the true temperature. By varying this fictitious temperature we can interpolate between choosing the system's most strongly-bonded clusters, when $T_f = T$, and choosing single particles, at infinite fictitious temperature. Thus one can propose moves which test the resilience of strong, but non-optimal interactions.

However, defining clusters according to bond energies results in an unphysical dynamics (see Appendix). To resolve this problem we can define clusters according to bond energy gradients by using a *dynamic* linking procedure. Here we introduce a cluster algorithm designed to evolve in an approximately physical manner a collection of strongly-attractive particles, and so permit the simulation of particles that spontaneously self-assemble. Such particles typically possess pairwise attractions of arbitrary strength, possibly very short range, and a high degree of angular specificity ('patchiness'). Our algorithm is a 'virtual-move' Monte Carlo (VMMC) scheme in which one particle first executes a 'virtual' trial move. We determine which of its neighbours move in a similar fashion by calculating bond energies before and after the proposed move. We iterate this procedure from all 'recruited' neighbours and stop when no more particles show a tendency to move. We then update simultaneously the positions of all affected particles.

This scheme evolves particles in a manner approximating realistic dynamics, while bypassing the need for the explicit computation of forces. Although this is in principle true of standard single-particle Monte Carlo schemes, the latter suffer a dramatic slowing-down in the presence of strong, short-ranged interactions. In addition, in the context of self-assembling systems, single-particle moves suppress in an unphysical manner possible modes of assembly (or, importantly, kinetic trapping) via the collision of multi-particle intermediates. The VMMC algorithm approximates the collective updates of particle positions characteristic of molecular dynamics simulations, whilst retaining the traditional advantages of the Monte Carlo approach. The latter include the ability to deal with pathological (e.g. perfectly sharp) potentials, and to employ a basic step size larger than that required by molecular dynamics simulations.

This paper is organised as follows. In Section II we show how one can avoid the unphysical kinetic traps that plague conventional MC cluster algorithms when applied to strongly-interacting particles. We illustrate this idea in Section III using a simple model system. In Sections IV and V we turn to dynamics. Although often regarded purely as a tool for obtaining equilibrium averages, a Monte Carlo simulation can in many cases approximate natural dynamics. In Section IV we describe the central result of this paper. We show that by proposing moves of particles based upon individual bond energy gradients, one can evolve in an approximately realistic (and computationally efficient) way a system of strongly-interacting particles. In Section V we apply this algorithm to a sys-

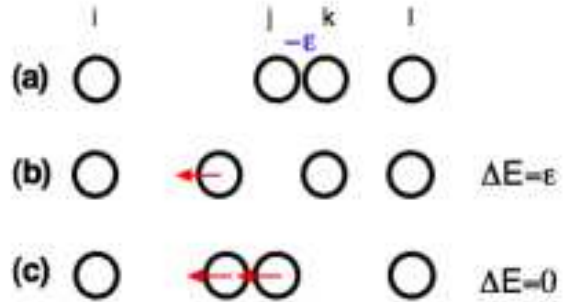


FIG. 1: An illustration of the difficulty encountered by standard Monte Carlo methods in the presence of very strong, short-ranged interactions. Here we show four pairwise-interacting particles, i , j , k and l . Only particles j and k interact, and do so with energy $\epsilon_{jk} = -\epsilon$, with $\epsilon \gg k_B T$. A natural dynamics would see particles j and k move in concert. A standard Monte Carlo scheme consists of sequential moves of individual particles. Any move of particle j which breaks the bond with particle k (**a** \rightarrow **b**) is rejected with a probability $1 - e^{-\epsilon/k_B T} \approx 1$; no significant motion of particles j or k is possible. The solution is to move particles j and k simultaneously (**a** \rightarrow **c**). We shall discuss different ways of choosing aggregates of particles to move in order to 1) avoid unphysical traps plaguing conventional Monte Carlo schemes, and 2) approximate physical dynamics.

tem of self-assembling components designed to model the aggregation of protein complexes called chaperonins. We conclude in Section VI.

II. AVOIDING UNPHYSICAL TRAPS IN CONVENTIONAL MC CLUSTER ALGORITHMS

In this section we show that a straightforward modification of existing MC cluster algorithms [11] can be used to evolve strongly-attractive particles without encountering unphysical kinetic traps. The scheme we describe is related to one proposed by Wu, Chander and Smit [13, 14]. Let us explain the idea with reference to Figure 2. Here we consider in d dimensions a system of N particles, each endowed with a hard-core radius a and a short-ranged, pairwise potential ϵ_{ij} . Shown is a typical cluster move (and its reverse) from state μ to state ν . We define two particles to be contiguous if their centres are separated by a distance less than or equal to $2a + a_0$, where a_0 is the interaction range of the potential. We define a *physical cluster* (abbreviated simply to 'cluster') as a group of contiguous particles. We shall use an iterative linking procedure, described below, to select a group of particles, \mathcal{C} . This group can range in size from a single particle to any one cluster in the system. We shall call this group of particles a *pseudocluster*. In Figure 2 the pseudocluster \mathcal{C} is shown in blue. We perform on \mathcal{C} either a rigid-body rotation about an arbitrary axis through its centre of mass, or a translation in an arbitrary direction.

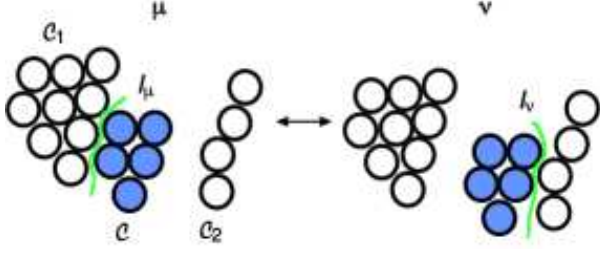


FIG. 2: An illustrative collective move. We define a pseudocluster \mathcal{C} (blue particles; see text), and subject it to a rotation or a translation. Here a proposed translation moves \mathcal{C} from contact with cluster \mathcal{C}_1 in state μ to contact with cluster \mathcal{C}_2 in state ν . The interface between the pseudocluster and its environment in state α is labelled I_α , and is defined by the set of all pairwise interactions between white and blue particles.

In the figure, one such translation happens to bring the pseudocluster into contact with the cluster \mathcal{C}_2 .

To define a pseudocluster \mathcal{C} we select from the system a ‘seed’ particle i . We form links between i and each particle j with probability

$$p_{ij} = \max \left(0, 1 - e^{\beta_f u_f(\epsilon_{ij})} \right). \quad (1)$$

This is a straightforward generalization of the form chosen by Swendsen and Wang [11]. Here β_f is a free parameter that we shall call the fictitious reciprocal temperature. The term $u_f(\epsilon_{ij})$ is a fictitious potential, and can be chosen for convenience. The simplest choice is to set the fictitious potential equal to the true potential. For some applications a convenient choice is $u_f(\epsilon) = \epsilon \Theta(r_0 - r)$: $u_f(\epsilon) = \epsilon$ within some cutoff distance r_0 , and zero otherwise. This renders potentials of arbitrary range amenable to the iterative linking scheme described below.

From each linked particle j we form links with probability $p_{jj'}$ to all particles j' not already linked to i . We iterate this procedure until no further links form. For a system with short-ranged interactions ϵ , or a system in which $u_f(\epsilon)$ is chosen to be short-ranged, each stage k of the iteration corresponds essentially to considering the k -th nearest neighbours of i .

Linking particles in the manner dictated by Equation (1) results in the pseudocluster \mathcal{C} (see Figure 2) being selected and moved with probability

$$W_{\text{gen}}(\mu \rightarrow \nu) = P_{\text{seed}}(\mu) P_{\text{build}}(\mathcal{C}; \mu) W_{\text{move}}(\mathcal{C}; \mu \rightarrow \nu). \quad (2)$$

Here $P_{\text{seed}}(\mu)$ accounts for the likelihood of choosing a seed particle in the pseudocluster \mathcal{C} . The factor $P_{\text{build}}(\mathcal{C}; \mu)$ returns the probability of building the pseudocluster \mathcal{C} in microstate μ , given that the seed particle has been chosen. It depends on two factors:

$$P_{\text{build}}(\mathcal{C}; \mu) = \prod_{\mathcal{I}_\mu} [1 - p_{ij}] \sum_{\mathcal{R}} \prod_{\langle ij \rangle_\ell} p_{ij}. \quad (3)$$

The product over the interface \mathcal{I}_μ is the likelihood that no links are formed between \mathcal{C} and its environment in

state μ . From (1), this product is equal to $e^{\beta_f U_\mu}$, where $U_\mu \equiv \sum_{\mathcal{I}_\mu} \min(0, u_f(\epsilon_{ij}))$ is the attractive part of the fictitious interfacial energy between the pseudocluster \mathcal{C} and its environment in state μ . The second factor in (3) is the probability of forming links $\langle ij \rangle_\ell$ between the constituent monomers of \mathcal{C} . In general there are many distinct realizations \mathcal{R} of links leading to the same chosen pseudocluster (denoted by $\sum_{\mathcal{R}}^{\mathcal{C}}$), and the product runs over links comprising one such realization. This piece is equal to the corresponding factor for the reverse move $\nu \rightarrow \mu$.

The third factor in (2), $W_{\text{move}}(\mathcal{C}; \mu \rightarrow \nu)$, is the rate for moving (translating and rotating) the pseudocluster \mathcal{C} , so that the system adopts microstate ν . Here we shall consider a uniform distribution of translations and rotations, in which case $W_{\text{move}}(\mathcal{C}; \mu \rightarrow \nu) = W_{\text{move}}(\mathcal{C}; \nu \rightarrow \mu)$.

Finally, we note that the internal cluster energies in states μ and ν are identical, and so the ratio of Boltzmann weights $\rho(\nu)/\rho(\mu)$ reduces to $e^{-\beta(E_\nu - E_\mu)}$, the exponential of the difference of the reduced interfacial energies between \mathcal{C} and its respective environments. Here $E_\alpha \equiv \sum_{\mathcal{I}_\alpha} \epsilon_{ij}$.

The generation rate for the reverse move $W_{\text{gen}}(\nu \rightarrow \mu)$ differs from its counterpart for the forward move (2) only in the product over the interface in P_{build} , and the factor $P_{\text{seed}}(\nu)$.

The concept of detailed balance ensures that a system evolves towards equilibrium by requiring that the rates W for passing between any two states μ and ν satisfy

$$\rho(\mu) W(\mu \rightarrow \nu) = \rho(\nu) W(\nu \rightarrow \mu). \quad (4)$$

Here $\rho(\alpha) = Z^{-1} e^{-\beta H_\alpha}$ is the Boltzmann weight with respect to the system’s Hamiltonian in state $\alpha \in \{\mu, \nu\}$, H_α ; $\beta \equiv 1/T$ is the reciprocal temperature (we adopt units such that $k_B = 1$); and Z is the partition function. The rates W will in general depend on the fictitious reciprocal temperature, β_f . Equation (4) ensures that detailed balance is respected *provided* that the distribution $Q(\beta_f)$ from which β_f is drawn is the same for both transitions $\mu \leftrightarrow \nu$.

The rate for passing between states is the product of the rates of proposing (generating) and of accepting such a move: $W(\mu \rightarrow \nu) = W_{\text{gen}}(\mu \rightarrow \nu) W_{\text{acc}}(\mu \rightarrow \nu)$. The ratio of acceptance rates satisfying detailed balance (4) is

$$\frac{W_{\text{acc}}(\mu \rightarrow \nu)}{W_{\text{acc}}(\nu \rightarrow \mu)} = \frac{\rho(\nu)}{\rho(\mu)} \frac{W_{\text{gen}}(\nu \rightarrow \mu)}{W_{\text{gen}}(\mu \rightarrow \nu)}. \quad (5)$$

This ratio can be evaluated for our particle-linking procedure:

$$\frac{W_{\text{acc}}(\mu \rightarrow \nu)}{W_{\text{acc}}(\nu \rightarrow \mu)} = \frac{P_{\text{seed}}(\nu)}{P_{\text{seed}}(\mu)} e^{-\beta(E_\nu - E_\mu) + \beta_f(U_\nu - U_\mu)}. \quad (6)$$

Henceforth we shall choose our seed particle with uniform probability. Provided that the number of particles N does not change, $P_{\text{seed}}(\alpha) = 1/N$, independent of the

state α . The ratio $P_{\text{seed}}(\nu)/P_{\text{seed}}(\mu)$ is then unity. For the move $\mu \rightarrow \nu$, we choose as the acceptance probability

$$p_{\text{acc}}(\mu \rightarrow \nu) = \min \{1, \exp(-\beta E_{\nu, \mu} + \beta_f U_{\nu, \mu})\}. \quad (7)$$

Here $E_{\nu, \mu} \equiv E_\nu - E_\mu$ and $U_{\nu, \mu} \equiv U_\nu - U_\mu$. Recall that E_α denotes the interfacial energy between pseudocluster \mathcal{C} and its environment in a given microstate, $E_\alpha \equiv \sum_{\mathcal{I}_\alpha} \epsilon_{ij}$, whereas $U_\alpha \leq 0$ denotes the *attractive part* of the *fictitious* energy between \mathcal{C} and its environment, $U_\alpha \equiv \sum_{\mathcal{I}_\alpha} \min(0, u_f(\epsilon_{ij}))$.

In the case where the inter-particle potential is attractive, $\epsilon_{ij} < 0$, and we choose a fictitious potential $u_f(\epsilon_{ij})$ equal to the true potential ϵ_{ij} , the procedure we have described is particularly straightforward to implement. Particles are linked according to a simple probability, $p_{ij} = 1 - e^{-\beta_f |\epsilon_{ij}|}$, and the ratio of acceptance rates is a simple function of the change in energy resulting from the move. For the move $\mu \rightarrow \nu$, the acceptance probability (7) reduces to

$$p_{\text{acc}}(\mu \rightarrow \nu) = \min \left(1, e^{(\beta_f - \beta)(E_\nu - E_\mu)}\right). \quad (8)$$

For infinite fictitious temperature, $\beta_f = 0$, the likelihood of forming links between the seed i and any other particle is zero, and so the algorithm executes single-particle moves with Metropolis acceptance probability $\min(1, e^{-\beta(E_\nu - E_\mu)})$. For a fictitious temperature equal to the true temperature, $\beta_f = \beta$, and for attractive interactions, the acceptance probability is unity.

By drawing a fictitious reciprocal temperature in the range $\beta_f \in [0, \beta]$, we can interpolate between single-particle moves and rejection-free cluster moves. In the following section we demonstrate the advantage offered by generalizing the rejection-free cluster algorithm to one possessing a lower acceptance rate, but, crucially, an improved *proposal* rate. When applied to a tightly-bound aggregate of particles, the rejection-free scheme does not allow the construction of pseudoclusters smaller than the aggregate. Thus the aggregate cannot relax through moves in concert of its constituents. In other words, the *generation* rate for many transitions involving the collective motion of tightly-bound particles is close to zero. By contrast, varying β_f allows one to increase markedly the generation rates of these moves, at the affordable cost of reducing slightly their acceptance rates. As a result, one can choose from the aggregate pseudoclusters of arbitrary size, and thus propose collective internal relaxations in the presence of arbitrarily strong interactions. We refer to this procedure as cluster ‘cleaving’.

In the following section we demonstrate the nature of the unphysical kinetic traps that the cleaving algorithm is designed to avoid. In Section IV we introduce a virtual-move Monte Carlo cluster algorithm designed to evolve such systems in an approximately realistic fashion.

III. AVOIDING KINETIC TRAPS ASSOCIATED WITH REJECTION-FREE MOVES

To visualize the nature of the kinetic traps the cluster cleaving algorithm is designed to avoid, we present data from Monte Carlo simulations of a system of pairwise-interacting particles. The system we study is chosen to be difficult to simulate using only single-particle techniques, namely a collection of strongly-interacting particles. Our chosen pair potential is a caricature of a Lennard-Jones interaction, and our system is a prototype of a dense, strongly-interacting aggregate. The strength of interaction need be only a few $k_B T$ before conventional MC single-particle or rejection-free cluster algorithms encounter unphysical kinetic traps. In our example we choose an interaction much stronger, to demonstrate that the cleaving algorithm can cope with arbitrarily strong interactions. Our aim is to demonstrate that it is beneficial to sacrifice an acceptance rate of unity for the freedom to propose moves that lead to productive relaxation of the system.

Our test system consists of 100 hard disks of diameter a in two dimensions, endowed with an attractive piecewise-linear pair potential of range a . With the inter-particle separation denoted by r , particles experience a hard-core repulsion for $r < a$. The potential increases linearly from its minimum, $\epsilon_0 = -45 k_B T$, at $r = a$ to $-15 k_B T$ at $r = 3a/4$. From $r = 3a/4$ to the potential increases linearly to zero at $r = 2a$. Thereafter, it is zero. This system possesses a thermodynamically stable ground state corresponding to an hexagonal close-packed sheet.

We can demonstrate the type of metastable structure that develops in the presence of the rejection-free cluster algorithm by ordering the system initially as a *square* lattice (with some positional disorder). We use a maximum step size of $a/10$. In Figure 3 we show a sequence of configurations obtained in this manner (time is measured in units of MC sweeps). On the left we show a sequence obtained using a mixture of single-particle moves and cluster moves in the the rejection-free limit, and on the right we show a sequence obtained using a mixture of single-particle moves and the cleaving algorithm (we show the most ‘successful’ example obtained from ten trajectories in each case). We find that relaxation is frustrated and that jammed structures persist for the single-particle moves in combination with rejection-free cluster moves. These jammed structures owe their existence to the following mechanism. First, potential energy gradients encourage neighbouring particles to aggregate into dense clumps separated by voids of lower density, a relaxation that can be accomplished readily by single-particle moves. Thereafter, because of the strength of the inter-particle contacts, the rejection-free cluster algorithm fails to propose moves of one clump relative to another. Since the structure does not readily relax in a single-particle fashion – the steeper gradient of the potential near its minimum disfavours the ‘jumping’ of single

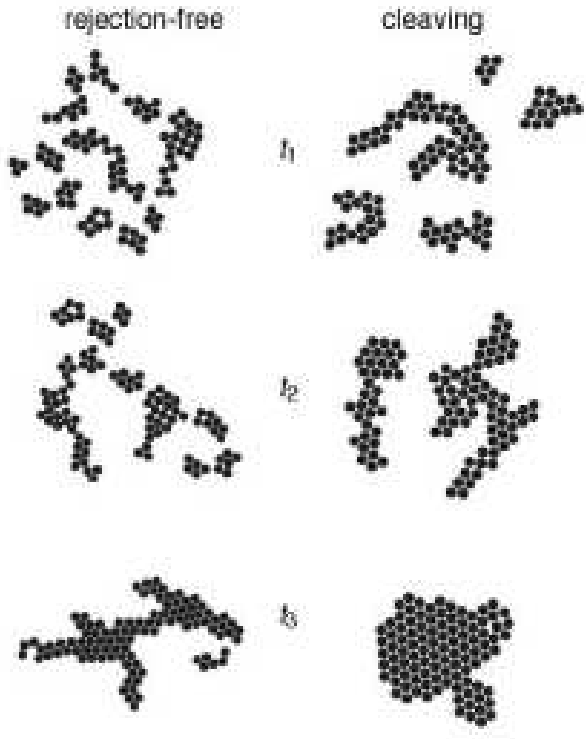


FIG. 3: Configurations from representative trajectories of our test system (see text) at times $t_1 < t_2 < t_3$. Left panels: single-particle moves plus rejection-free cluster algorithm, leading to a configuration trapped far from equilibrium. Right panels: single-particle moves plus cleaving algorithm. The latter circumvents the unphysical kinetic traps associated with rarely testing strong inter-cluster bonds.

particles across a gap – the system finds itself in an unphysical kinetic trap. The unphysical nature of this trap results from the rejection-free cluster algorithm’s inability to test the resilience of inter-clump contacts that are large compared with $k_B T$. Structures of this nature relax very slowly via single-particle moves.

The cleaving algorithm can circumvent this trap. For sufficiently large T_f all contacts, regardless of strength, are tested. Here we draw the fictitious reciprocal temperature from a uniform distribution between 0 and β , i.e. $Q(\beta_f) = \beta^{-1} \Theta(\beta - \beta_f)$, and we use a fictitious potential

$$u_f(\epsilon) = \begin{cases} \epsilon & (\epsilon \leq \epsilon_0 + \delta_\epsilon) \\ 0 & (\epsilon > \epsilon_0 + \delta_\epsilon) \end{cases}. \quad (9)$$

Here $\delta_\epsilon = 0.1 k_B T$ is a cutoff energy. The fictitious potential (9) returns the true energy ϵ if ϵ is within a tolerance δ_ϵ of the potential minimum, ϵ_0 , i.e. if $-45 k_B T \leq \epsilon \leq -44.5 k_B T$. If ϵ is outside this range, the fictitious potential returns zero. This ensures that only those particles which are optimally bound undergo significant collective translations or rotations.

The variation in fictitious temperature allows the algorithm to propose moves of any clump relative to any

other, and the system can relax via collective moves of its constituents. However, the cleaving algorithm is not immune to the *physical* kinetic traps associated with the rearrangement of a dense structure: in some simulations of the type discussed above we observe very slow equilibration even using the cleaving algorithm. There exist algorithms better suited to studying the equilibrium properties of dense structures [9, 25]. Our aim in this section was to illustrate how unphysical traps can be avoided by sacrificing acceptance rate for the freedom to propose moves able to relax the system.

In the following section we introduce a dynamic cluster-moving algorithm.

IV. A DYNAMIC CLUSTER-FORMING PROCEDURE

Self-assembly is the process whereby interacting components organize spontaneously into thermodynamically stable patterns or aggregates. It is the means by which many biological structures form, from the protein packaging of viruses [22, 23] to the lipid membranes enclosing cells. The self-assembly of nanometer-scale objects constitutes an important branch of nanotechnology.

In studying self-assembly, it is important to identify the nature of the inter-component interactions that can lead to stable structures with the required symmetry. However, a full understanding of how assembly is effected requires a characterization of its dynamics. Binding that depends on the precise alignment of neighbouring components might ensure thermodynamic stability, but the time required for two bodies to collide in this manner could be prohibitively long. Similarly, very strong contacts contribute to the stability of equilibrium structures but could also transiently stabilize malformed aggregates, thereby impeding equilibration.

Brownian dynamics is perhaps the most natural kinetic model for several examples of biological self-assembly, given the relatively large sizes and small diffusivities of many proteins. However, component-component interactions take place on a timescale many orders of magnitude less than assembly of overall structures. As aggregation proceeds, productive rearrangements increasingly require the concerted motion of many components. If the steric constraints of each body are to be preserved, the simulation time step must remain much smaller than the timescale of this motion. Integrating equations of motion under such conditions is a very costly way to update the system.

While the cluster cleaving algorithm we have presented is not plagued by this problem, neither does it evolve a self-assembling system in a manner in accord with natural dynamics. The reason for this deficiency is that clusters are moved according to bond *energies*, not energy *gradients*. In the Appendix we show analytically that this scheme corresponds to an unrealistic dynamics in which a particle’s drift velocity is not simply propor-

tional to the negative of the potential energy gradient it experiences.

In this section we shall introduce our central result, a virtual-move cluster algorithm. This algorithm is designed to approximate physical dynamics by moving interacting bodies either individually or in concert according to individual bond energy gradients. This procedure may be regarded as the dynamic generalization of the link-forming procedure described in Section II, or as a particle-based adaptation of the Wolff cluster algorithm [12]. It is similar in some respects to the algorithm described in [9], but differs in that here proposed moves are chosen to correspond as closely as possible to realistic particle displacements.

The essence of the scheme is as follows. We start in state μ . We select a ‘seed’ particle i uniformly, and assign to this seed a move *map*. This map defines a random translation or rotation, and thus defines a notional new state, ν . We execute a ‘virtual’ move of the seed under this map, and look to those particles $\{j\}$ with which it interacted in state μ . We link each particle j to the seed with a probability $p_{ij}(\mu \rightarrow \nu)$ that depends on the energy of the relevant bond before *and after* the move of the seed:

$$p_{ij}(\mu \rightarrow \nu) = \begin{cases} \max(0, 1 - e^{\beta E_c(i,j) - \beta E_I(i,j)}) & (E_c < E_0) \\ 0 & (E_c \geq E_0) \end{cases} \quad (10)$$

Here

$$E_c(i,j) \equiv \epsilon_{ij}(x'_i, x'_j) = \epsilon_{ij}(x_i, x_j) \quad (11)$$

is the energy of the bond ij following a *collective* virtual move of i and j (where each move according to the same map). Because the map defines either a rigid-body rotation or a translation, the particles do not move relative to each other, and so this bond energy is identical to that in the starting state μ . This gives rise to the second equality in Equation (11). The term

$$E_I(i,j) = \epsilon_{ij}(x'_i, x_j) \quad (12)$$

is the bond energy following an individual virtual move of i , and no move of j (the bond energy in the proposed state ν). With probability p_{ij} we move i and j in concert, according to the specified move map. With the complementary probability we move i but not j . This is the key difference from a standard single-particle MC scheme: here, if the move of particle i relative to j is rejected, i and j are instead moved in concert.

The energy E_0 is a cutoff energy. If the initial bond energy E_c is less favourable than this cutoff energy then we do not attempt to link the two particles sharing the bond. We shall see later that we must account separately, via the overall acceptance rate, for particles between which we attempted no link ($E_c \geq E_0$) but which suffered an increase in their bond energy following the move.

If a link is formed, the linkee particle adopts the move map of the seed, ensuring that these move together in

a rigid-body fashion. The seed is then returned to its original position. We continue this scheme hierarchically, attempting to link each linked particle to any unlinked particle with which it interacts, and stop when no further links form. We then update simultaneously the positions of all linked particles. In this way particles explore their potential energy gradients without the need for the explicit computation of forces.

The scheme is best explained using an example, which we show in Figure 4. We consider five particles, i , j , k , l and m , endowed with short-ranged, orientation-dependent pairwise interactions (particle orientations not shown). Bonds ij , ik and jk are strong, possessing a large negative energy ϵ , while bond kl is weak, possessing an energy of interaction $\delta \approx 0$. There is no interaction between m and any other particle.

We first choose a seed particle, say i . To i we assign a move map, denoted by a red arrow. The map here defines a rightward translation. We shall denote the state of particle α by $x_\alpha = \{\mathbf{r}_\alpha, \mathbf{S}_\alpha\}$ (which contains the position \mathbf{r}_α and orientation \mathbf{S}_α of the particle). After executing its virtual move, the state of particle α becomes $x'_\alpha = \mathcal{U}_{x_\alpha} x_\alpha$, where \mathcal{U}_{x_α} encodes the map in question. For translations the map \mathcal{U}_{x_α} is independent of x_α . For rotations we choose an arbitrary axis through the centre of mass of the seed particle; \mathcal{U}_{x_α} effects rotations about this axis.

To determine whether i moves individually or in concert with other particles, we form links between i and each particle with a probability given by Equation (10). In Section V we consider only attractive interactions, and so we shall take a cutoff energy $E_0 = 0$: we attempt links only between particles that interacted prior to their attempted move. If two particles having no interaction in state μ possess a positive energy following their move (which in Section V means an overlap), we reject the move (see later). We shall retain the symbol E_0 for generality. For systems with long-ranged interactions one can make the cutoff E_0 more discriminating, e.g. $E_0 = -k_B T$, or distance-dependent, ensuring linking attempts only between neighbouring particles.

In our example the linking procedure unfolds as follows. We assign to i a virtual move map (**a**). We test its link with j , and so consider only these particles. We calculate the initial energy of the bond ij , E_c , and find it to be large and negative $E_c = \epsilon \ll 0$ (**b**). We move i under its map and calculate the new energy of the bond (**c**). Because attractions are short-ranged we find this energy to be zero. We propose a link between i and j with probability $p_{ij} = 1 - e^{\beta \epsilon} \approx 1$. In our example this link is accepted, and so j adopts the move map of i . The latter is returned to its original position (**d**). We next propose a link between i and k , and find that it is also accepted (**e**).

All particles interacting with i have now been tested. As before, we iterate the link-forming procedure: we propose links between particles linked to i and particles with which these particles interact. Here that means testing

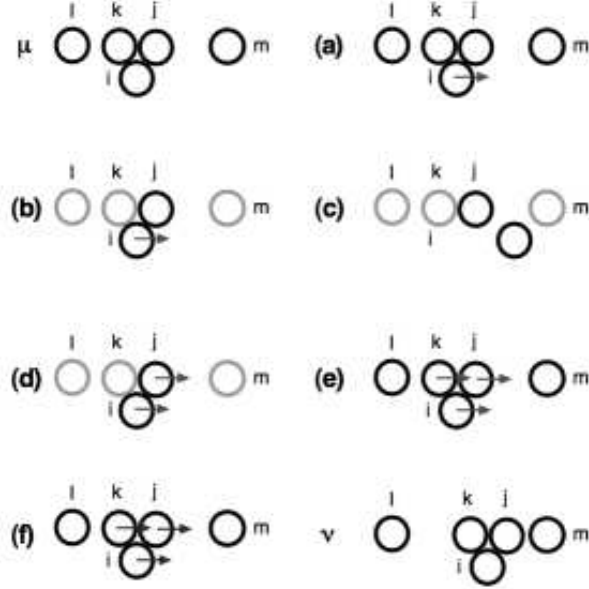


FIG. 4: An illustration of the virtual-move Monte Carlo algorithm. From starting state μ the seed particle i is assigned a virtual move map, denoted by a red arrow (a). We propose a link between i and j by calculating the energy difference of the bond ij before and after the virtual move of i (b, c). In this example a link forms, and j adopts the virtual move map of i ; the latter is returned to its original position (d). We iterate this procedure until no more links form (e), and displace all linked particles simultaneously (blue arrows denote real, not virtual, moves): (f) $\rightarrow \nu$. The new configuration ν is proposed as the final state, and the Monte Carlo acceptance probability is evaluated.

the interaction kl ; this weak bond is linked with probability $p_{kl} \approx \delta/k_B T \approx 0$. In our example this link is not formed. The virtual-move linking procedure is now finished. The final virtual moves are adopted as real moves (red arrows become blue arrows, panel (f)) and all particles in the chosen pseudocluster (i, j, k) are displaced simultaneously, according to their map ν . We propose this state ν as the final state, and evaluate the Monte Carlo acceptance factor.

The acceptance probability for the virtual-move procedure can be evaluated from Equations (5), (2), (3) and (10). We refer again to Figure 2 as an illustration of a general move from a state μ to a state ν . We choose the seed particle uniformly from any in the system, giving $P_{\text{seed}}(\mu) = P_{\text{seed}}(\nu)$. Unlike in the static case, the probability of forming links between particles such that the blue cluster is the chosen pseudocluster depends on whether one is executing the forward or reverse move, and so does not cancel from Equation (5). We write as $\sum_{\mathcal{R}} P_{\text{gen}}^{\mathcal{R}}(\mathcal{C}|\mu \rightarrow \nu)$ the probability of generating the internal links of pseudocluster \mathcal{C} given that one is proposing a move from state μ to state ν , summed over all realizations \mathcal{R} of links. We shall delay evaluation of this factor until the end. The remaining quotient in Equation (5)

concerns the probability of *not* forming links between the pseudocluster and its environment in each state. Equation (5) reduces to

$$\frac{W_{\text{acc}}(\mu \rightarrow \nu)}{W_{\text{acc}}(\nu \rightarrow \mu)} = e^{-\beta(E_{\nu} - E_{\mu})} \frac{\prod_{\nu \rightarrow \mu} q_{ij}(\nu \rightarrow \mu)}{\prod_{\mu \rightarrow \nu} q_{ij}(\mu \rightarrow \nu)} \times \frac{\sum_{\mathcal{R}} P_{\text{gen}}^{\mathcal{R}}(\mathcal{C}|\nu \rightarrow \mu)}{\sum_{\mathcal{R}} P_{\text{gen}}^{\mathcal{R}}(\mathcal{C}|\mu \rightarrow \nu)}. \quad (13)$$

The first factor on the right-hand side of Equation (13) is the ratio of the Boltzmann weights of the two states. As before, the energy E_{α} is the interfacial energy between the cluster and its environment in state α . The second factor denotes the link-breaking probabilities $q_{ij} \equiv 1 - p_{ij}$. The product $\prod_{\mu \rightarrow \nu}$ runs over all links which must *not* form in order to move from state μ to state ν . The second line of Equation (13) concerns the probability of generating links such that \mathcal{C} is the selected pseudocluster.

Next we evaluate the link-breaking factors. Consider a move from state μ to state ν . The probability of *not* linking a particle j (that is not a member of the chosen pseudocluster) to a particle i (a member of the pseudocluster) is, from Equation (10),

$$q_{ij}(\mu \rightarrow \nu) = \begin{cases} \min\left(1, e^{\beta\epsilon_{ij}^{(\mu)} - \beta\epsilon_{ij}^{(\nu)}}\right) & (\epsilon_{ij}^{(\mu)} \leq E_0) \\ 1 & (\epsilon_{ij}^{(\mu)} \geq E_0) \end{cases}. \quad (14)$$

The product of all such unformed links gives us

$$\prod_{\mu \rightarrow \nu} q_{ij}(\mu \rightarrow \nu) = \prod_{\langle ij \rangle_{\text{p.i.}}} \min\left(1, e^{\beta\epsilon_{ij}^{(\mu)} - \beta\epsilon_{ij}^{(\nu)}}\right), \quad (15)$$

where $\langle ij \rangle_{\text{p.i.}}$ denotes all blue-white pairs which interacted with an energy more favourable than the cutoff energy *prior* to their move: $\epsilon_{ij}^{(\mu)} < E_0$ (the subscript p.i. means ‘previously interacting’). Recall that we shall take the cutoff $E_0 = 0$ later; we retain the symbol for generality. The factor corresponding to (15) for the reverse move follows by interchanging the labels μ and ν . Hence we have

$$\frac{\prod_{\nu \rightarrow \mu} q_{ij}(\nu \rightarrow \mu)}{\prod_{\mu \rightarrow \nu} q_{ij}(\mu \rightarrow \nu)} = \prod_{\langle ij \rangle'} e^{\beta\epsilon_{ij}^{(\nu)} - \beta\epsilon_{ij}^{(\mu)}}. \quad (16)$$

where $\langle ij \rangle'$ denotes all blue-white pairs *except* those whose bond energies in state μ are ‘noninteracting’ according to the cutoff criterion ($\epsilon_{ij}^{(\mu)} \geq E_0$), and move uphill in energy ($\epsilon_{ij}^{(\nu)} > \epsilon_{ij}^{(\mu)}$). For negative interactions and cutoff $E_0 = 0$, the latter criterion is true only in the presence of particle overlap.

Inserting (16) in Equation (13) gives us

$$\frac{W_{\text{acc}}(\mu \rightarrow \nu)}{W_{\text{acc}}(\nu \rightarrow \mu)} = \prod_{\langle ij \rangle_{\text{p.n.}}} e^{-\beta(\epsilon_{ij}^{(\nu)} - \epsilon_{ij}^{(\mu)})} \times \frac{\sum_{\mathcal{R}} P_{\text{gen}}^{\mathcal{R}}(\mathcal{C}|\nu \rightarrow \mu)}{\sum_{\mathcal{R}} P_{\text{gen}}^{\mathcal{R}}(\mathcal{C}|\mu \rightarrow \nu)}. \quad (17)$$

The link-breaking factors have cancelled the ratio of Boltzmann bond weights, *except* those corresponding to particle-pairs $\langle ij \rangle_{\text{p.n.}\uparrow}$ that interact in state μ with an energy less favourable than the cutoff, *and* move uphill in energy (the subscript p.n. \uparrow means ‘previously noninteracting particles whose bond has increased in energy’, where ‘noninteracting’ is defined according to the cutoff criterion).

Lastly we must evaluate the second line of Equation (17). In contrast to the static case, the probability of generating links such that \mathcal{C} is the chosen pseudocluster differs for the forward and reverse moves. Consider Figure 5. Here we show a starting configuration, μ , of three particles, i , j and k . Let us say that we try to generate a new state (‘forward’ move, \mathbf{f}) by displacing i to the right. The proposed position of i overlaps with j and k , and so according to Equation (10) we form links ij and ik with unit probability. The cluster ijk moves rightward as a rigid body.

But now we encounter a problem generating the reverse move. Displacing k to the left (move \mathbf{r}') will displace i with unit probability, but j will move with a probability depending on its energies of interaction with i and k . Likewise, displacing i to the left (‘reverse’ move \mathbf{r}) will cause j and k to move with a probability in general less than one. If one accepts the forward move with unit probability, then there is in general no way to engineer the reverse move with the probability required to ensure balance.

The solution is to modify the acceptance rates of the forward and reverse moves so that balance is restored. We define a forward move as a proposed move from state μ to state ν , given a seed particle, a move map for the seed particle, and a particular realization \mathcal{R} of links. Because linking is a dynamic procedure, \mathcal{R} must include the direction in which the links were formed (e.g. from i to j , or from j to i), and not just which links were formed. We define the reverse move as a proposed transition from state ν to state μ , given the same seed particle, the move map of the forward transition with sign inverted (for translations and rotations), and the same realization \mathcal{R} (pattern and direction) of links. When proposing the forward move, we form a link between two particles i and j with probability $p_{ij}(\mu \rightarrow \nu)$, as discussed. Here the linker particle moves according to the forward move map. As we do so, we perform a ‘reverse’ virtual move of the linker particle and record the probability that the link ij would form were the linker particle translating (or rotating) in the opposite direction, $\hat{p}_{ij}(\nu \rightarrow \mu)$. We then suppress the forward move by the product over all links of the quotient $\hat{p}_{ij}(\nu \rightarrow \mu)/p_{ij}(\nu \rightarrow \mu)$.

In the example shown in Figure 5, the forward move \mathbf{f} is initiated by displacing the seed i rightwards. Links ij and ik form with certainty, and so we do not propose a link between k and j . The probability that these links would have formed had the seed moved leftward (reverse move \mathbf{r}) is $1 - e^{-\beta \Delta E_{i\alpha}}$, $\alpha \in \{j, k\}$, where $\Delta E_{i\alpha}$ is the change in binding energy between i and α . We therefore

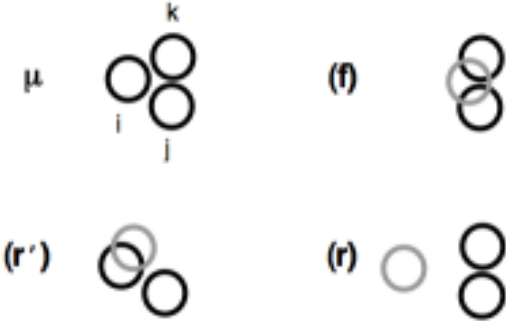


FIG. 5: Ensuring reversibility for cluster moves. We require that the likelihood of a given particle, say i , ‘pushing’ (\mathbf{f}) and ‘pulling’ (\mathbf{r}) its host cluster is identical. To do so, every time we link two particles we record the likelihood that the link would have formed had the reverse move been proposed. In the reverse move, the linking particle translates in the opposite direction (or rotates with the opposite sense). We account for this probability difference via the overall acceptance rate, ensuring superdetailed balance. The acceptance rate for such ‘avalanche’ moves is high if the binding energy of particles is high (the regime of interest), and vanishes in the limit of vanishing interaction strength [26].

suppress the likelihood of the forward move by a factor $(1 - e^{-\beta \Delta E_{ij}})(1 - e^{-\beta \Delta E_{ik}})$. For strong attractions (the regime in which we are interested) this factor is close to unity; for hard particles with no attractions it is zero, and we must reject the forward move. We thus ensure that the probability of a given particle ‘pushing’ or ‘pulling’ its host cluster is identical.

Detailed balance is therefore enforced by accepting the moves $\mu \leftrightarrow \nu$ with relative rates

$$\frac{W_{\text{acc}}(\mu \rightarrow \nu)}{W_{\text{acc}}(\nu \rightarrow \mu)} = \prod_{\langle ij \rangle_{\text{p.n.}\uparrow}} e^{-\beta(\epsilon_{ij}^{(\nu)} - \epsilon_{ij}^{(\mu)})} \times \frac{\sum_{\mathcal{R}}^{\mathcal{C}} \prod_{\langle ij \rangle_{\ell}}^{\mathcal{R}} \hat{p}_{ij}(\nu \rightarrow \mu)}{\sum_{\mathcal{R}}^{\mathcal{C}} \prod_{\langle ij \rangle_{\ell}}^{\mathcal{R}} p_{ij}(\mu \rightarrow \nu)}. \quad (18)$$

Here $\prod_{\langle ij \rangle_{\ell}}^{\mathcal{R}}$ runs over one particular realization \mathcal{R} of links $\langle ij \rangle_{\ell}$, and $\sum_{\mathcal{R}}^{\mathcal{C}}$ runs over all realizations of links such that \mathcal{C} is the chosen pseudocluster. For large systems it is not feasible to enumerate all possible ways of generating a given pseudocluster. Instead, we use the virtual move algorithm to determine one particular realization of links, and compute the likelihood that each of these links will form in the reverse direction. We then accept the forward move with a probability equal to the minimum of unity

and the right-hand side of

$$\frac{W_{\text{acc}}(\mu \rightarrow \nu | \mathcal{R})}{W_{\text{acc}}(\nu \rightarrow \mu | \mathcal{R})} = \prod_{\langle ij \rangle_{\text{p.n.}\uparrow}} e^{-\beta(\epsilon_{ij}^{(\nu)} - \epsilon_{ij}^{(\mu)})} \times \prod_{\langle ij \rangle_{\ell}}^{\mathcal{R}} \frac{\hat{p}_{ij}(\nu \rightarrow \mu)}{p_{ij}(\mu \rightarrow \nu)}. \quad (19)$$

This is the condition of superdetailed balance [3]: by enforcing Equation (19) for *any* given realization of links, we ensure that the probabilities of moving from μ to ν and back again are such that we ensure the correct equilibrium distribution.

The first factor in Equation (19) can be simplified if we consider a cutoff $E_0 = 0$. In this case we propose no links between particles which have a non-attractive interaction, and Equation (19) reduces to

$$\frac{W_{\text{acc}}(\mu \rightarrow \nu | \mathcal{R})}{W_{\text{acc}}(\nu \rightarrow \mu | \mathcal{R})} = \prod_{\langle ij \rangle_{\text{p.n.}\uparrow}} e^{-\beta\epsilon_{ij}^{(\nu)}} \prod_{\langle ij \rangle_{\ell}}^{\mathcal{R}} \frac{\hat{p}_{ij}(\nu \rightarrow \mu)}{p_{ij}(\mu \rightarrow \nu)}. \quad (20)$$

We take as the acceptance rate $W_{\text{acc}}(\mu \rightarrow \nu | \mathcal{R})$ the minimum of unity and the right-hand side of Equation (20). Here the product $\prod_{\langle ij \rangle_{\text{p.n.}\uparrow}}$ runs over pairs which did not interact in state μ but possess positive energy in state ν . We consider in Section V particles with purely attractive interactions and hard-core repulsions. In this case, barring overlaps no particle can have positive energy, and the first factor on the right-hand side of (20) is unity. If particles overlap, the first factor on the right-hand side of (20) is zero, and we reject the move. For general systems, ‘soft’ overlaps of particles are rejected probabilistically.

The second product on the right-hand side of Equation (20) runs over one particular realization \mathcal{R} of links. It can be thought of as a means of ensuring that the probability of a given particle ‘pushing’ a cluster is the same as its probability of ‘pulling’ the same cluster (or for rotations, ensuring an equal likelihood of effecting a rigid-body rotation in clockwise and anticlockwise directions), and is required to enforce balance. This factor approaches unity when for strongly-bound particles: multi-particle displacements occur with high probability. The factor becomes small for particles attracting weakly, indicating that whole-cluster displacements are unlikely. In this regime, however, single-particle moves experience little slowing-down, and the need for a cluster algorithm is reduced.

Returning to our earlier example, Figure 4, we see that the only contribution to the first factor of the acceptance criterion (20) comes from bond jm (because in state μ this bond is ‘noninteracting’ according to the cutoff criterion). The new energy of bond jm is certainly less than or equal to zero, because no overlap has occurred; the first factor is therefore unity. Considering the second factor of Equation (20), we see that if the trimer ijk possesses a large binding energy the proposed collective displacement is likely to be accepted. In this case we accept state ν with high probability.

As defined, the algorithm does not update the positions of all particles with equal frequency. Because collective moves can in principle be initiated from any particle, those particles residing in large clusters have a greater chance of changing position than do isolated particles. We account for this by suppressing the rate for moves of clusters of size n by a factor of $1/n$. It is not efficient to engineer this suppression via the acceptance rate. *A priori* we do not know how many particles will be assigned to a pseudocluster. We could waste much effort by building pseudoclusters only to reject their move. Instead, we suppress the *generation* rate of such moves. We draw a random real number $\xi \in [0, 1]$, and define a cluster cutoff $n_c \equiv \sup(\xi)$. We then abort the link formation procedure if the pseudocluster size exceeds n_c . In this way we ensure (with reasonable computational efficiency) that particles experience positional updates with approximately equal frequency, a requirement necessary for dynamical fidelity.

One strength of the virtual-move scheme is that it allows one to identify groups of particles that move in concert, and to suppress their displacement in order to approximate hydrodynamic damping. A body moving in an overdamped fashion through a fluid possesses translational and rotational diffusion properties that depend on its size and shape. These properties cannot be fully captured by considering only individual or pairwise interactions between the cluster’s constituent particles.

Stokes’ law states that a cluster of effective hydrodynamic radius R (a measure of the greatest extent of the cluster perpendicular to the direction of motion) possesses a translational diffusion constant $3D_t(R) = \Gamma R^{-1}$, and a rotational diffusion constant $8D_r(R) = \Gamma R^{-3}$, where $\Gamma \equiv k_B T(\pi\eta_w)^{-1}$; $\eta_w \approx 10^{-3}$ Pa s is the viscosity of water. We can respect this damping within the virtual-move algorithm by calculating for the chosen pseudocluster its effective hydrodynamic radius R , where

$$R^2 = \langle |(\mathbf{r}_i - \mathbf{r}_c) \times \hat{\mathbf{n}}|^2 \rangle. \quad (21)$$

The average $\langle \cdot \rangle \equiv n^{-1} \sum_{i=1}^n$ runs over all of the n particles i (having coordinates \mathbf{r}_i) comprising the pseudocluster. The vector $\hat{\mathbf{n}}$ is either the direction of translation or the axis of rotation, as appropriate; the vector \mathbf{r}_c is for rotations the position of the centre of rotation, and for translations the centre of mass $\langle \mathbf{r}_i \rangle$ of the diffusing pseudocluster. This size- and shape-dependent drag becomes increasingly important when the system in question is composed of very polydisperse or anisotropic aggregates.

We enforce this damping by suppressing cluster displacements by a factor $\sqrt{\mathcal{D}_\gamma(R)}$, where $\gamma \in \{t, r\}$ for a translation or rotation as required. We set $\mathcal{D}_t(R) = R_0/R$, (R_0 being the monomer radius), and $\mathcal{D}_r(R) = (R_0/R)^3$. Combining the results of this section, our final

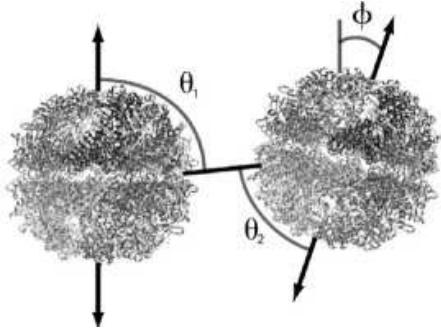


FIG. 6: Geometry for a schematic model of chaperonin self-assembly [16, 17, 18]. We use a short-ranged, anisotropic pair potential to mimic the tendency of chaperonins to bind equator-to-equator. We show chaperonin structure determined by homology together with the angles relevant for our chosen interaction. The angle between orientation vectors is ϕ ; the angles between orientation vectors and the inter-unit separation vector are θ_1 and θ_2 .

acceptance rate is

$$W_{\text{acc}}(\mu \rightarrow \nu | \mathcal{R}) = \sqrt{D_\gamma(R)} \min \left\{ 1, \prod_{\langle ij \rangle_{\text{p.n.}}} e^{-\beta \epsilon_{ij}^{(\nu)}} \times \prod_{\langle ij \rangle_e} \frac{\hat{p}_{ij}(\nu \rightarrow \mu)}{p_{ij}(\mu \rightarrow \nu)} \right\}. \quad (22)$$

Note that we also employ the ‘early rejection’ scheme discussed above. This scheme effects a suppression of the *generation* rate of moves of clusters of size n by a factor of $1/n$, ensuring that all particles move with approximately equal frequency.

This completes our discussion of the the key result of this paper, the virtual-move Monte Carlo scheme. By forming links according to individual bond energies before *and after* a proposed move, we displace particles according to individual bond energy gradients without calculating forces explicitly. We ensure that particles are updated with approximately equal frequency, and we damp the movement of multi-particle clusters in order to respect Stokes’ law. In the following section we apply this algorithm to a model of biological self-assembly.

V. APPLICATION TO SELF-ASSEMBLY

In the presence of ATP and magnesium ions, the heat shock protein (Hsp60) from the organism *Sulfolobus shibatae* self-assembles in two stages. First, monomers (‘sub-units’) of the protein assemble into 18-membered, nearly-spherical complexes (‘units’) of radius 17 nm. Next, units aggregate into extended structures often microns in scale. We refer to the 18-membered complexes as, interchangably, ‘units’ or ‘chaperonins’. Experiments with the wild-type protein lead to two distinct types of chaperonin super-structures under subtly different external

conditions: two-dimensional sheets with a high degree of hexagonal order, and quasi one-dimensional strings. We focus here on assembly into sheets, the control of which provides a means of engineering organic templates with a high degree of order, potentially useful for electronics devices. Free-floating sheets are also formed by the self-assembly of inorganic nanocrystals [27].

Computer models can help reveal the range of inter-unit attraction strength and specificity required to effect large-scale self-assembly [28, 29]. The detailed interactions between chaperonins are not known. Patterns of polar, nonpolar and charged amino acid side chains exposed by individual chaperonins do not immediately suggest specific regions where two units would strongly bind, nor do experimental results over a range of ionic strength clarify the physical nature of the binding interaction. It is clear, however, that forces between sheet-forming chaperonins favour equatorial contact [31]. We can exploit this information when constructing a simple model of chaperonin self-assembly.

We build such a model by coarse-graining over the microscopic details of individual units (we consider units to be stable against dissociation into protein monomers). The simplest such approximation is to regard units as spheres without surface detail [30]. We mimic the effect of the microscopic unit-unit interactions by endowing spheres with a short-ranged, anisotropic pair potential designed to encourage mutual equatorial contact.

Figure 6 illustrates the geometry of our chosen potential. Each sphere has a polar orientation vector, shown as a double-headed arrow (we assume ‘up-down’ symmetry). We also assume azimuthal symmetry, so that the pair potential does not change if spheres are rotated about their orientation vector (chaperonin units possess 9-fold rotational symmetry about their polar axis). We choose the attraction to be strong if neighbouring orientation vectors are aligned ($\phi = 0, \pi$), and perpendicular to the inter-unit separation vector ($\theta_{1,2} = \pi/2, 3\pi/2$). Thus we allow only binding between complementary regions (equator-to-equator), and do not allow, for example, equator-to-pole binding. This reflects the near-perfect alignment observed between chaperonins in sheet-like assemblies, and also the notable absence of disordered aggregates [31].

Analytically, our chosen potential is

$$\epsilon(\mathbf{r}) = -J_{\text{eq}} \Theta(R_{\text{max}} - \hat{r}) \hat{\mathcal{C}}_1(\phi) \mathcal{C}_0(\theta_1) \mathcal{C}_0(\theta_2). \quad (23)$$

The step function Θ ensures that two spheres interact only when their surfaces are separated by a distance less than R_{max} , which we shall vary between $R_0/4$ and $R_0/8$, R_0 being the chaperonin radius. Here $\hat{r} \equiv r - 2R \geq 0$ is the distance between the surfaces of neighbouring chaperonins. For $\hat{r} < 0$ we assume a hard-core repulsion. We parameterize the angular interaction via the ‘cooperativity’ function $\mathcal{C}_\alpha(\psi) \equiv e^{-(\cos \psi - \alpha)^2/\sigma^2}$, which rewards an angle ψ if its cosine is within some tolerance (specified by a parameter σ) of the value α . The symmetrized cooperativity function $\hat{\mathcal{C}}_\alpha(\psi) \equiv \mathcal{C}_\alpha(\psi) + \mathcal{C}_{-\alpha}(\psi)$ rewards values

of $\cos \psi$ near $\pm \alpha$. The first angular factor in (23) encourages the alignment of neighbouring units; the second and third angular factors encourage mutual equatorial contact. We vary σ between 0.2 and 0.4.

Here we demonstrate that the virtual-move algorithm (incorporating hydrodynamic damping) described in Section IV can identify several distinct mechanisms of sheet assembly. These range from monomer addition onto a single nucleus, to the binding and merging of separate sheet-like structures. The latter mechanism, which turns out to be a plentiful source of kinetic ‘traps’, is not accessible to conventional single-particle MC methods. We focus here on typical mechanisms of assembly for our model system, and leave a detailed quantitative study of the rates of aggregation as a function of attraction parameters for elsewhere.

By assuming a chaperonin radius of $R_0 = 9$ nm, we obtain from Stokes’ law a translational diffusion constant for chaperonin monomers of $D_t(R_0) \approx 5 \times 10^{-11} \text{ m}^2 \text{s}^{-1}$ (compare the self-diffusion coefficient of water, $D_{\text{H}_2\text{O}} \approx 5 \times 10^{-9} \text{ m}^2 \text{s}^{-1}$). We draw monomer displacements Δ from a uniform distribution with extrema $\pm 0.9R_0$ [32]. From these data we calculate that our monomer displacement timescale corresponds to approximately 10^{-8} s. Thus a Monte Carlo sweep of 1000 particles equates to roughly 10^{-5} s. We fix the relative rates of translation and rotation by imposing Stokes’ law for monomers, namely $3D_t(R_0) = 8R_0^2 D_r(R_0)$. We ran simulations for $\sim 10^5$ to $\sim 10^7$ MC sweeps, and so probe timescales of order 1 to 100 seconds. In experiments [16, 17, 18], large-scale assembly is observed on timescales of minutes to hours. Thus we expect our dynamic simulations to detect at least the onset of significant chaperonin self-assembly.

We start from an initial state consisting of 1000 monomers randomly dispersed and oriented in a three dimensional simulation box. We impose periodic boundaries in each dimension. Units comprised about 0.8 % by volume of the simulation box, equivalent to a protein concentration of about 5 mg/ml (experimental concentrations of protein range between 1 and 5 mg/ml [31]). We then evolve the system according to the virtual-move scheme with hydrodynamic damping. Times are quoted in virtual-move Monte Carlo sweeps, with one VMMC sweep corresponding to the (uniform) choice of 1000 seed particles.

In Figure 7 we present a ‘kinetic phase diagram’ of chaperonin assembly, obtained using single VMMC trajectories. We vary interaction strength J_{eq} and inverse angular specificity σ . For interaction ranges $R_{\text{max}} = R_0/4$ (top panel) and $R_{\text{max}} = R_0/8$ (bottom panel), we indicate where we find ‘no assembly’ (open red squares), ‘good assembly’ (blue circles) and ‘bad assembly’ (closed red squares). We define the largest time accessed at each phase point, the ‘end’ of the trajectory, as t_{end} . We conclude that ‘no assembly’ has taken place if the largest cluster at time t_{end} possesses fewer than 15 chaperonin units. For those systems for which this is not true,

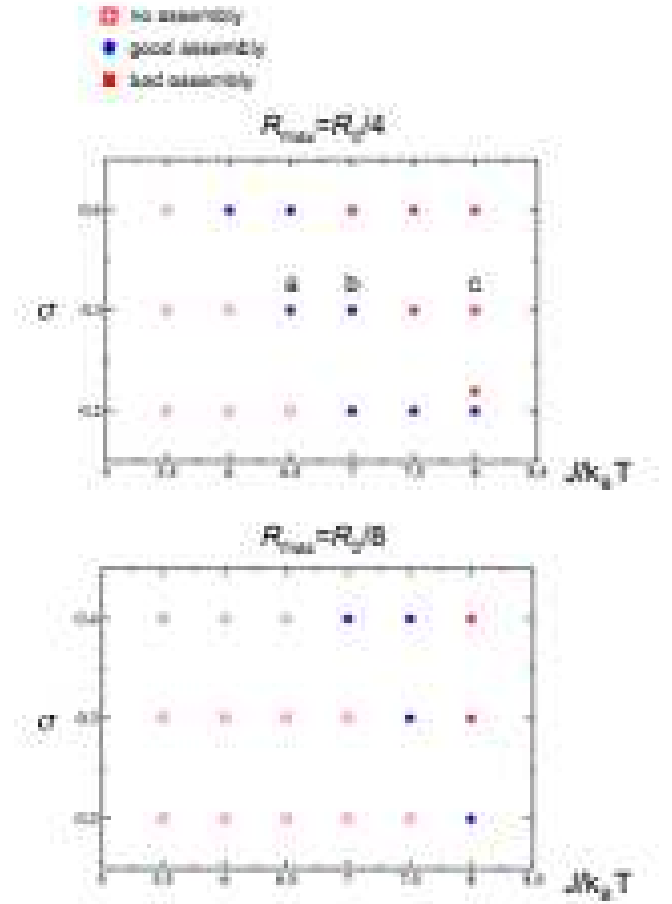


FIG. 7: Kinetic phase diagram for our schematic chaperonin system, evolved using the VMMC algorithm with hydrodynamic damping. We indicate regions of ‘no assembly’ (open red squares), ‘good assembly’ (blue circles) and ‘bad assembly’ (closed red squares); see text. A good assembly-bad assembly pair indicates that intermediate building blocks are well-formed, but subsequent multi-particle collisions induce kinetic frustration. Configurations corresponding to phase points **a**, **b** and **c** are shown in Figures 8 to 10.

we conclude that assembly is ‘good’ if the constituent monomers of the largest cluster in the system possess on average more than 4.75 ‘bonds’. We define a particle’s bond number as its energy divided by the equatorial coupling, J_{eq} . We conclude that assembly is ‘bad’ if, at t_{end} , the system’s largest cluster possesses more than than 15 members, but fewer than 4.75 bonds per member.

For those phase points exhibiting bad assembly, we identify the largest number of bonds possessed by members of the largest cluster at *any* time along the trajectory. If this number is greater than 4.75, we plot a ‘good assembly-bad assembly’ symbol pair at that phase point. This indicates that while the intermediate building blocks may at some time in the trajectory be well-formed, collisions between these multi-particle structures eventually

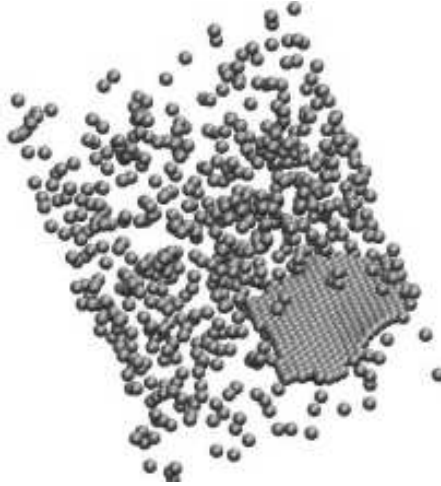


FIG. 8: Configuration obtained after 3.5×10^6 VMMC sweeps for our schematic chaperonin system of spheres with sticky equators of strength $J_{\text{eq}} = 6.5 k_{\text{B}}T$ (phase point **a** of Figure 7). At this attraction strength nucleation is sufficiently rare that self-assembly proceeds by the binding of monomers to a single sheet. The resulting structure is relatively well-formed.

give rise to an aggregate that is ill-formed.

A note on timescales: ideally, we would present in a kinetic phase diagram data obtained at fixed Monte Carlo time. Here that is not feasible, because of the broad distribution of relaxation times observed in our chaperonin system. For example, at phase point ($R_{\text{max}} = R_0/4, J_{\text{eq}} = 8 k_{\text{B}}T, \sigma = 0.4$) we observe the development of a simulation box-spanning cluster in $\sim 10^5$ VMMC sweeps. After an equal time, phase point ($R_{\text{max}} = R_0/4, J_{\text{eq}} = 6.4 k_{\text{B}}T, \sigma = 0.3$) exhibits no appreciable assembly (nucleation is very slow). After 10^6 VMMC sweeps, however, the latter system is well assembled (see below). Consequently, we show data at fixed processor times ($t_{\text{end}} \sim 5.5 \times 10^5$ s), such that we judged assembly at all phase points to be sufficiently far advanced that the ultimate fate of each system is clear. This criterion is clearly arbitrary. However, we argue that the mechanisms of assembly revealed in this manner are qualitatively robust to variations in the criteria used to draw the kinetic phase diagrams.

The general trend of assembly revealed in Figure 7 indicates that regions of good assembly occupy a relatively small volume of phase space. This volume is defined by a balance between collision rates (controlled largely by density, attraction range and the specificity parameter σ) and relaxation rate (controlled largely by J_{eq}), such that assembled structures form rapidly enough to be observed on the timescales simulated ('good assembly', blue circles), but not so rapidly that they malform. If this optimal ratio is disturbed, we observe over-rapid growth leading to malformed structures ('bad assembly', closed red squares), or growth too slow to be observed on the timescales simulated ('no assembly', open red squares).

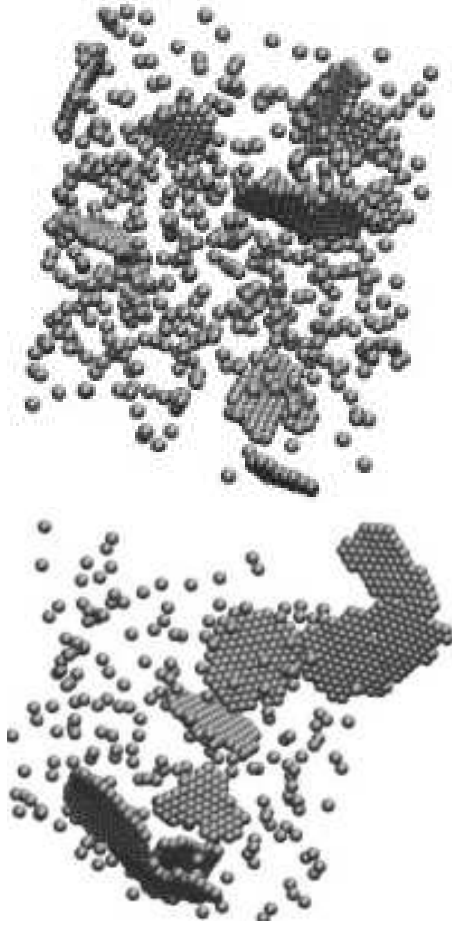


FIG. 9: Configurations obtained using the VMMC algorithm applied to the chaperonin system with equatorial interaction strength $J_{\text{eq}} = 7 k_{\text{B}}T$ (phase point **b** of Figure 7). A modest increase in attraction strength promotes nucleation to a considerable degree. Assembly proceeds both by the addition of monomers to single sheets (top panel, $\sim 0.2 \times 10^6$ sweeps), and via collisions of multi-particle sheets (bottom panel, $\sim 0.5 \times 10^6$ sweeps). Sheets often collide awkwardly, producing ill-formed structures. Here relaxation of these structures is sufficiently rapid that assembly is still 'good'.

At one phase point we see initially good assembly, where monomers bind into small, well-formed sheets, followed by bad assembly induced by sheets colliding awkwardly and producing malformed structures. The rate of sheet collision is set by Stokes' law, which is respected by the VMMC algorithm. Reducing the attraction range (upper panel to lower panel) has the effect of reducing collision frequency. We observe an offsetting and a narrowing of the region of good assembly.

It is illuminating to examine the assembly mechanisms observed as we vary only the equatorial coupling, exemplified by phase points **a**, **b** and **c** in the top panel of Figure 7. In Figure 8 (phase point **a** of Figure 7) we show a late-time configuration for units possessing equatorial coupling $J_{\text{eq}} = 6 k_{\text{B}}T$. Assembly proceeds, following a rare nucleation event, via the binding of monomers to a

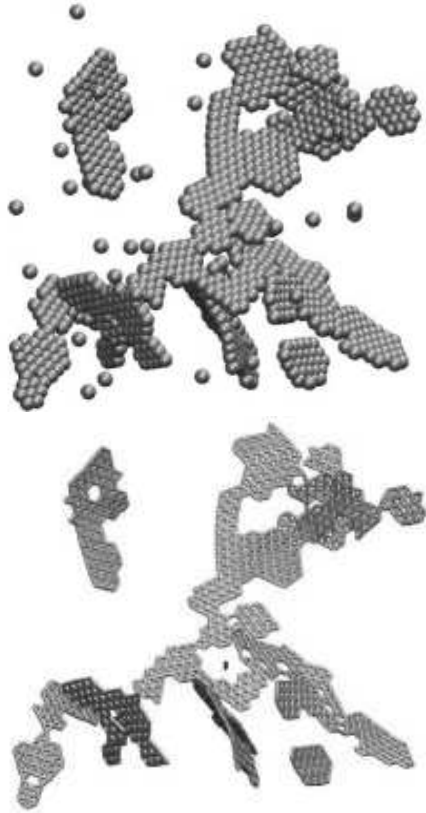


FIG. 10: Configuration obtained via VMMC for our schematic chaperonin system with equatorial interaction strength $J_{\text{eq}} = 8 k_{\text{B}}T$ (phase point **c** of Figure 7). Nucleation is so rapid that multi-particle binding events occur frequently. The resulting structures fail to relax before encountering other such structures, leading to aggregates trapped far from equilibrium. Top: excluded-volume view. Bottom: bond view.

single sheet-like nucleus. The resulting structure is well-formed and defect-free. The crossover from non-assembly to assembly is rather sharp: at the concentrations used, we observed no assembly within our simulation time at equatorial attraction strength $J_{\text{eq}} = 5.5 k_{\text{B}}T$.

The change in assembly mechanism caused by increasing the unit-unit interaction strength is dramatic. At a slightly larger interaction strength, $J_{\text{eq}} = 7 k_{\text{B}}T$ (Figure 9; phase point **b** of Figure 7), nucleation proves more rapid. Assembly proceeds via the organization of monomers into multiple sheets. These sheets diffuse according to Stokes' law, and collide with each other. Multi-particle collisions are often awkward, providing an ill-formed template to which monomers bind. In the example shown, however, relaxation is sufficiently rapid that large structures can relax via large-lengthscale fluctuations: assembly is still 'good'.

At still higher attraction strengths, such as $J_{\text{eq}} = 8 k_{\text{B}}T$ (Figure 10; phase point **c** of Figure 7), aggregation is so rapid that nuclei do not have time to relax into low energy sheet-like structures before they bind to other such ill-formed aggregates. In this regime assembly

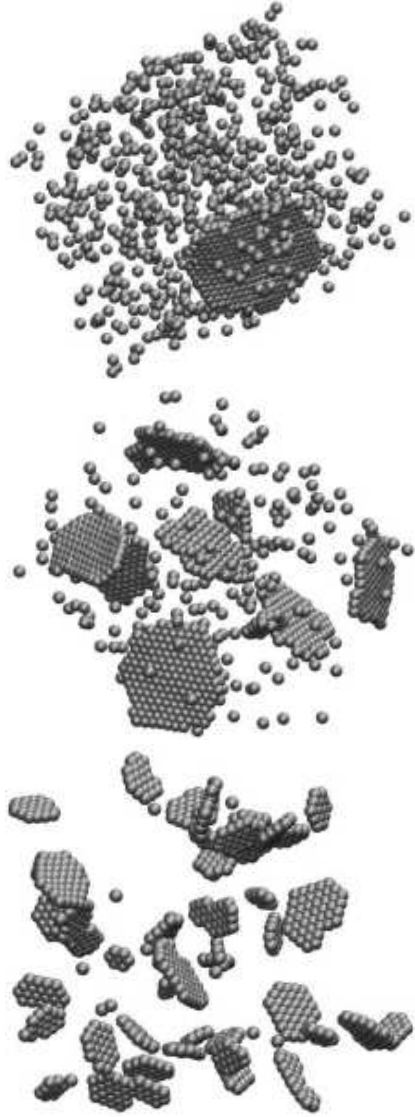


FIG. 11: Configurations obtained via a single-particle Monte Carlo algorithm for our schematic chaperonin system with $R_{\text{max}} = R_0/4$, $\sigma = 0.3$ and (top to bottom) equatorial interactions $J_{\text{eq}} = 6.5, 7$ and $8 k_{\text{B}}T$. Stokes' law is violated by single-particle moves (large clusters essentially do not move), and very few multi-particle collisions take place. For all attraction strengths structures are well-formed, even though VMMC results indicate that for the two larger values of J_{eq} a dynamics satisfying Stokes' law results in the formation of non-optimal aggregates via multi-particle collisions (see Figures 8 to 10).

is frustrated kinetically.

These results indicate that the assembly mechanism for our schematic chaperonin model changes considerably with the unit-unit attraction strength. Because these interactions are angularly specific, particles must collide equator-to-equator in order to bind. For insufficiently strong equatorial attractions, random collisions between monomers do not result in stable intermediates, and no assembly is seen. For sufficiently strong attrac-

tions, assembly proceeds via the binding of monomers to a single sheet-like nucleus. Aggregates grown in this way are typically well-formed and defect-free. Increasing unit-unit couplings beyond this point slows equilibration. Nucleation is promoted, and collisions between multiple sheet-like nuclei, which occur with a frequency governed by Stokes' law, usually result in awkwardly-bound structures that relax only slowly. There exists a narrow regime of phase space in which structures formed in this way can relax, via collective fluctuations, into an approximation of a well-assembled sheet. However, at very large attraction strengths nucleation is so rapid that the nuclei themselves are ill formed, leading to disordered aggregates.

We note in passing that single-particle Monte Carlo techniques suppress unphysically the diffusion of multi-particle structures. When interactions are such that appreciable clustering of particles develops, the dynamics of a system evolved according to single-particle Monte Carlo protocols does not satisfy Stokes' law. As a result, the source of kinetic traps whereby clusters collide and bind awkwardly is removed. In Figure 11 we show configurations generated by single-particle translations and rotations applied to systems corresponding to the interaction parameters of Figures 8, 9 and 10 (phase points **a**, **b** and **c** of Figure 7). For all three attraction strengths single-particle moves generate well-formed, isolated clusters. For an attraction strength of $J_{\text{eq}} = 6.5 k_{\text{B}}T$ the VMMC results indicate that the ratio of the rates of cluster growth and diffusion is such that single-particle addition to a single nucleus is the dominant assembly mechanism; single-particle moves naturally capture this dynamics. However, for the larger attraction strengths a dynamical protocol satisfying Stokes' law generates multi-particle collisions, inducing a degree of kinetic frustration that increases with attraction strength. Single-particle moves fail to identify this mechanism. Note that if inter-component interactions are such that assembly must proceed via the interaction of multi-particle structures [23], single-particle moves would encounter an unphysical kinetic trap.

VI. CONCLUSIONS

We have presented a virtual-move Monte Carlo cluster algorithm designed to permit the collective relaxation of particles possessing attractions of arbitrary strength, range and geometry, an important example being self-assembling particles endowed with strong, short-ranged and angularly specific ('patchy') attractions. By calculating pair energies before and after notional virtual moves, we deduce whether particles move individually or in concert. Using an 'early rejection' scheme designed to suppress moves of clusters by a factor inversely proportional to the cluster size, we ensure that all particles move with approximately equal frequency. We also ensure that Stokes' law is satisfied for aggregates of arbitrary size

and shape. Our scheme approximates the simultaneous updates of particle positions characteristic of molecular dynamics simulations. Its advantage over the latter lies in the fact that by computing energies before and after virtual moves, one bypasses the need to compute forces explicitly. In addition, one can propose particle displacements larger than the width of the potential well, regardless of the depth of that well. We expect that this algorithm can be used to study the phase behaviour and aggregation mechanisms of a variety of self-assembling systems.

Acknowledgments

We thank Edward H. Feng, Matthew B. Francis, Michael Hagan, Robert L. Jack, Chad D. Paavola, Sander Pronk and Jonathan D. Trent for important discussions. The similarity in name between our algorithm and the virtual-move parallel tempering scheme of Ref. [33] is due to our lack of imagination.

VII. APPENDIX: MONTE CARLO DYNAMICS

A. Single-particle moves

A Monte Carlo simulation consisting of a sequence of moves of individual particles can in many cases approximate natural dynamics. As a simple example, consider a collection of particles in one dimension in a potential $U(r)$. For sufficiently small step size Δ , a Metropolis Monte Carlo trajectory is equivalent to the behaviour described by a diffusive Fokker-Planck equation [5, 6].

Let us demonstrate this equivalence for a single particle with coordinate r in a potential $U(r)$. The master equation for the particle's motion is

$$\begin{aligned} \partial_t P(r; t) &= \int_{r'} P(r'; t) W(r' \rightarrow r) \\ &\quad - \int_{r'} P(r; t) W(r \rightarrow r'). \end{aligned} \quad (24)$$

Here $\int_{r'} \equiv \int_{r-\Delta}^{r+\Delta} dr'$, $P(r; t)$ is the probability of finding the particle at position r at time t , and $W(r \rightarrow r')$ is the rate for moving from position r to position r' . For a Metropolis acceptance rate the latter reads

$$W(r \rightarrow r') = W_0 W_{\text{gen}}(\delta r) \min \left(1, e^{-\beta [U(r') - U(r)]} \right). \quad (25)$$

The parameter W_0 is a reference frequency, and $W_{\text{gen}}(\delta r) = (2\Delta)^{-1}$ the *a priori* probability for choosing from a uniform distribution a step $\delta r \equiv r' - r$ in the range $[-\Delta, \Delta]$. The 'min' term encodes the Metropolis acceptance probability.

For a sufficiently small Δ one can expand Equation (24) in powers of $\hat{r} \equiv r' - r$. This is most easily done by changing the W notation from $W(r' \rightarrow r)$

to $W(r + \hat{r}; -\hat{r})$. The latter symbol means the rate for passing from configuration $r + \hat{r}$ ($= r'$) to configuration $r + \hat{r} - \hat{r} = r$, and can be expanded in its first argument: $W(r + \hat{r}; -\hat{r}) = W(r; -\hat{r}) + \hat{r} \partial_r W(r; -\hat{r}) + \dots$. Likewise, $P(r', t) = P(r, t) + \hat{r} \partial_r P(r, t) + \dots$. To second order in ∂_r , Equation (24) reads

$$\partial_t P(r; t) \approx \partial_r (\langle \hat{r} \rangle P(r, t)) + \frac{1}{2} \partial_r^2 (\langle \hat{r}^2 \rangle P(r, t)), \quad (26)$$

with

$$\langle \hat{r}^k \rangle \equiv \int_{-\Delta}^{\Delta} d\hat{r} \hat{r}^k W(r; -\hat{r}). \quad (27)$$

The derivative-free term $\int_r P(r, t) W(r; \hat{r}) - \int_{r'} P(r, t) W(r; -\hat{r})$ vanishes by symmetry. Equation (26) is a Fokker-Planck equation with drift velocity $v = -\langle \hat{r} \rangle$ and diffusion constant $D = \langle \hat{r}^2 \rangle$. Using Equation (25) we have to first order in \hat{r}

$$W(r; -\hat{r}) \approx \frac{W_0}{2\Delta} \min(1, 1 + \beta \hat{r} U'(r)). \quad (28)$$

We have assumed that $\hat{r}|U'(r)| \ll 1$. This is not true for a pathological potential such as (23), which possesses infinite gradients, but physically this is not a concern: the behaviour of a model with a ‘regularized’ potential (in which the step function is replaced by a sharp linear ramp) is similar to that of (23).

The integrals (27) can be evaluated in a piecewise fashion, with the minimum function in Equation (28) returning its first argument when $\hat{r} \geq 0$, and its second argument when $\hat{r} < 0$. To second order in Δ one can calculate that the drift velocity is proportional to the potential gradient, $v = -(\beta/6)\Delta^2 W_0 U'(r)$, and that the diffusion constant is $D = \Delta^2 W_0 / 3$. This corresponds to Langevin dynamics satisfying an Einstein (fluctuation-dissipation) relation $-v/D = (\beta/2)U'(r)$. This result is straightforwardly generalized to many particles and higher dimensions. Note that normally v is independent of temperature T (not $\propto \beta$ as here), and $D \propto T$ (not independent of T). This can be arranged by making the fundamental attempt frequency W_0 proportional to T [6].

Thus Monte Carlo moves of single particles in a potential take place in a dynamically realistic way. As discussed in this paper, problems arise when such potentials become sufficiently strong and short-ranged that the basic step size must be made inconveniently small in order to prevent acceptance rates from vanishing. Long timescales result. The algorithms we have introduced remedy this problem. In the remainder of this Appendix we shall show that the cluster cleaving algorithm, which forms pseudoclusters by linking particle pairs according to their *energies*, corresponds to an unphysical dynamics (a dynamics in which the drift velocity is not simply proportional to the potential gradient), and so should be regarded only as a scheme for obtaining equilibrium averages. By contrast, the VMMC algorithm, which links particle pairs in a manner consistent with their potential energy *gradients*, corresponds to an approximation of realistic dynamics.

B. Cluster cleaving algorithm

Here we consider the dynamics of the cleaving algorithm described in Section II. We use a fictitious potential equal to the true potential. Let us consider the separation vector x_{ij} between two particles i and j , which interact with an attractive pair potential $\epsilon_{ij}(x_{ij}) \leq 0$. The separation vector x_{ij} depends explicitly only on the pairwise energy by which i and j interact.

For the cleaving algorithm, the master equation for the coordinate x_{ij} is

$$\begin{aligned} \partial_t P(x_{ij}; t) &= \int_{\hat{x}} P(x'_{ij}; t) W_c(x_{ij} \rightarrow x'_{ij}; \beta_f) \\ &\quad - \int_{\hat{x}} P(x_{ij}; t) W_c(x_{ij} \rightarrow x'_{ij}; \beta_f). \end{aligned} \quad (29)$$

Here $\int_{\hat{x}} \equiv \int Q(\beta_f) d\beta_f \int_{-\Delta}^{\Delta} d\hat{x}$, where $\hat{x} \equiv x'_{ij} - x_{ij}$; $P(x_{ij}; t)$ is the probability of observing a bond separation x_{ij} at time t ; and $W_c(x_{ij} \rightarrow x'_{ij}; \beta_f)$ is the rate at which the cleaving move changes the bond separation from x_{ij} to x'_{ij} .

The rate W_c at which the separation x_{ij} changes follows straightforwardly from Equations (1) and (8). We assume that either particle i or particle j is chosen as a seed, and displaced by the vector \hat{x} . Then the bond separation x_{ij} changes if 1) *no* link is proposed between i and j , and 2) the Monte Carlo acceptance probability is satisfied. Condition 1) occurs according to Equation (1) with probability $\min(1, \exp\{\beta_f \epsilon_{ij}(x_{ij})\}) = \exp\{\beta_f \epsilon_{ij}(x_{ij})\}$. Criterion 2) is satisfied with a likelihood equal to the right-hand side of Equation (8). Hence

$$\begin{aligned} W_c(x_{ij} \rightarrow x'_{ij}) &= (2\Delta)^{-1} W_0 \exp\{\beta_f \epsilon_{ij}(x_{ij})\} \\ &\quad \times \min\left(1, e^{-(\beta - \beta_f)[\epsilon_{ij}(x'_{ij}) - \epsilon_{ij}(x_{ij})]}\right). \end{aligned} \quad (30)$$

Once again, W_0 is a reference frequency, and again we can expand the master equation (29) to second order in the small displacement Δ . We obtain the Fokker-Planck equation

$$\begin{aligned} \partial_t P(x_{ij}; t) &\approx - \partial_{x_{ij}} (v_{\text{eff}} P(x_{ij}; t)) \\ &\quad + \frac{1}{2} \partial_{x_{ij}} (D \partial_{x_{ij}} P(x_{ij}; t)), \end{aligned} \quad (31)$$

with effective drift velocity

$$v_{\text{eff}} = v - \frac{1}{2} \partial_{x_{ij}} D. \quad (32)$$

The ‘bare’ drift velocity v is

$$v = -\frac{\Delta^2}{6} \hat{W} \cdot (\beta - \beta_f) \partial_{x_{ij}} \epsilon_{ij}(x_{ij}), \quad (33)$$

and the diffusion constant is

$$D = \frac{\Delta^2}{3} \hat{W}. \quad (34)$$

Here we have defined the position-dependent rate

$$\hat{W} = W_0 \int Q(\beta_f) d\beta_f e^{\beta_f \epsilon_{ij}(x_{ij})}, \quad (35)$$

which contains an integral over β_f (this integral acts on any β_f -dependent factors to its right). By virtue of the position-dependence of (35), the effective drift velocity is not simply proportional to the negative of the potential gradient. Instead, it is biased by a term depending on the exponent of the local bond energy:

$$v_{\text{eff}} = -\frac{\Delta^2}{6} W_0 \beta [\partial_{x_{ij}} \epsilon_{ij}(x_{ij})] \int Q(\beta_f) d\beta_f e^{\beta_f \epsilon_{ij}(x_{ij})}. \quad (36)$$

This is unphysical. The cleaving algorithm evolves the system according only to an approximation of true Langevin dynamics: a particle's drift velocity is not simply proportional to the potential gradient it experiences, nor is the diffusion constant (34) independent of position. Only in the (undesirable) limit of single-particle moves, $Q(\beta_f) = \delta(\beta_f)$, is physical dynamics restored. Note also that in the conventional rejection-free limit, $Q(\beta_f) = \delta(\beta_f - \beta)$, drift and diffusion are both suppressed by a factor $e^{\beta \epsilon_{ij}(x_{ij})}$, demonstrating that in the limit of strong attractions little motion is possible.

The root of these difficulties is the fact that pseudoclusters are built according to pair energies, and not energy gradients. However, drift and diffusion still satisfy the required Einstein relation for evolution to equilibrium,

$$-\frac{v_{\text{eff}}}{D} = \frac{\beta}{2} \partial_{x_{ij}} \epsilon_{ij}(x_{ij}). \quad (37)$$

C. VMMC algorithm

Next we turn to VMMC algorithm described in Section IV. With similar notation to before, the master equation for the separation x_{ij} between particles i and j

is

$$\begin{aligned} \partial_t P(x_{ij}; t) &= \int_{\hat{x}} P(x'_{ij}; t) W_v(x'_{ij} \rightarrow x_{ij}) \\ &\quad - \int_{\hat{x}} P(x_{ij}; t) W_v(x_{ij} \rightarrow x'_{ij}), \end{aligned} \quad (38)$$

where $\int_{\hat{x}} \equiv \int_{-\Delta}^{\Delta} d\hat{x}$. The rate W_v (the subscript stands for ‘virtual’) at which the separation x_{ij} changes follows from Equation (10). We assume that the virtual displacement of particles i relative to j results in a change in the bond separation x_{ij} by \hat{x} . This change is accepted if 1) *no* link is proposed between i and j , and 2) the Monte Carlo acceptance probability is satisfied. Condition 1) occurs according to Equation (10) with probability

$$q_{ij}(x_{ij} \rightarrow x'_{ij}) = \min(1, \exp\{\beta \epsilon_{ij}(x_{ij}) - \beta \epsilon_{ij}(x'_{ij})\}). \quad (39)$$

If condition 1) is satisfied then condition 2) is automatically true provided that no particle overlaps occur. Thus

$$W_v(x_{ij} \rightarrow x'_{ij}) = \frac{W_0}{2\Delta} q_{ij}(x_{ij} \rightarrow x'_{ij}). \quad (40)$$

An expansion of Equation (38) in powers of Δ yields a Fokker-Planck equation with a physically realistic drift velocity

$$v = -\frac{\Delta^2}{6} W_0 \beta \partial_{x_{ij}} \epsilon_{ij}(x_{ij}), \quad (41)$$

and a constant diffusion parameter

$$D = \frac{\Delta^2}{3} W_0. \quad (42)$$

Provided that particles execute updates with approximately equal frequency, as described in Section IV, this scheme corresponds to an approximation of realistic dynamics.

[1] V.I. Manousiouthakis and M.W. Deem, *J. Chem. Phys.* **110**, 2753 (1999).
[2] O. Narayan and A. P. Young, *Phys. Rev. E* **64**, 021104 (2001).
[3] D. Frenkel, *Proc. Natl. Acad. Sci. USA*, **101** 51 (2004).
[4] D. Frenkel and B. Smit, *Understanding Molecular Simulation* (second edition), Academic Press (2002).
[5] K. Kikuchi, M. Yoshida, T. Maekawa and H. Watanabe, *Chem. Phys. Lett.* **185** 335 (1991).
[6] G. Tiana, L. Sutto and R.A. Broglia, *q-bio.0T/0606038* (2006).
[7] L. Berthier and W. Kob, *cond-mat/0610235* (2006).
[8] J.M. Romero-Enrique, L.F. Rull and A.Z. Panagiotopoulos *Phys. Rev. E* **66** 041204 (2002).
[9] J. Liu et al. *Phys. Rev. E* **71** 066701 (2005); J. Liu and E. Luijten, *Phys. Rev. Lett.* **92** 035504 (2004).
[10] G. Orkoulas and A.Z. Panagiotopoulos, *Fluid Phase Equilibria* **93** 223 (1993); *J. Chem. Phys.* **101**, 1452, (1994).
[11] R.H. Swendsen and J.-S. Wang, *Phys. Rev. Lett.* **58** 86 (1987).
[12] U. Wolff, *Phys. Rev. Lett.* **62**, 361 (1989).
[13] D. Wu, D. Chandler and B. Smit, *J. Phys. Chem.* **96** 4077 (1992).
[14] The static cluster-linking scheme and the method described in [13] are similar in the sense that both construct clusters according to the properties of particles (respectively, bond energies or degree of proximity) in the *initial* state. The virtual-move algorithm of Section IV defines clusters according to bond energies in the initial and proposed final states.
[15] K. Binder, Applications of the Monte Carlo Method in

Condensed Matter Physics, Springer, Berlin (1984).

[16] R.A. McMillan, C.D. Paavola, J. Howard, S.L. Chan, N.J. Zaluzec and J.D. Trent, *Nature Materials* **1**, 247 (2002).

[17] J.D. Trent, H.K. Kagawa, T. Yaoi, E. Olle, and N.J. Zaluzec, *Proc. Natl. Acad. Sci. USA* **94**, 5383 (1997).

[18] M.J. Ellis M, S. Knapp, P.J.B. Koeck, Z. Fakoor-Biniaz, R. Ladenstein and H. Hebert, *J. Struct. Biol.* **123**, 30 (1998).

[19] M.A. Horsch, Z. Zhang and S.C. Glotzer, *Phys. Rev. Lett.* **95**, 056105 (2005).

[20] Z. Zhang, M.A. Horsch, M.H. Lamm and S.C. Glotzer, *Nano Lett.* **3** (10), 1341 (2003).

[21] Z. Zhang and S.C. Glotzer, *Nano Lett.* **4** (8), 1407, (2004).

[22] D.C. Rapaport, *Phys. Rev. E.* **70**, 051905 (2004)

[23] M.F. Hagan and D. Chandler, *Biophys. J.* **91**, 42 (2006).

[24] F. Wang and D.P. Landau, *Phys. Rev. Lett.* **86**, 2050 (2001).

[25] C. Mak, *J. Chem. Phys.* **122** 21, 214110 (2005).

[26] W. Krauth, Statistical Mechanics: Algorithms and Computations, Oxford Master Series in Physics (2006).

[27] Z. Tang, Z. Zhang, Y. Wang, S.C. Glotzer and N.A. Kotov, *Science* **314** 5797, 274 (2006).

[28] A.M. Wilber, J.P. Doye, A.A. Louis, E.G. Noya, M.A. Miller and P. Wong, pre-print cond-mat/0606634 (2006).

[29] Z.-L. Zhang, A.S. Keys, T. Chen and S.C. Glotzer, *Langmuir* **21**, 25:11547 (2005).

[30] J. Harte, Consider a spherical cow. University Science Books (1988).

[31] C.D. Paavola, S.L. Chan, Y. Li, K.M. Mazzarella, R.A McMillan and J.D. Trent, *Nanotechnology* **17**, 1171 (2006).

[32] At the densities we consider, this step size is below the value at which kinetics and thermodynamics become biased; see M. Rottereau, J.C. Gimel, T. Nicolai and D. Durand, *Eur. Phys. J. E* **18**, 15 (2005).

[33] Coluzza, I. & D. Frenkel, *Chem. Phys. Chem.* **6** 9, 1779 (2005)

This figure "J_7_pic1.jpg" is available in "jpg" format from:

<http://arxiv.org/ps/cond-mat/0508100v5>

This figure "J_8_pic1.jpg" is available in "jpg" format from:

<http://arxiv.org/ps/cond-mat/0508100v5>

This figure "J_7_pic2.jpg" is available in "jpg" format from:

<http://arxiv.org/ps/cond-mat/0508100v5>

This figure "J_8_pic2.jpg" is available in "jpg" format from:

<http://arxiv.org/ps/cond-mat/0508100v5>

This figure "J_65.jpg" is available in "jpg" format from:

<http://arxiv.org/ps/cond-mat/0508100v5>

This figure "chap_diagram.jpg" is available in "jpg" format from:

<http://arxiv.org/ps/cond-mat/0508100v5>

This figure "hold_em_illustration.png" is available in "png" format from:

<http://arxiv.org/ps/cond-mat/0508100v5>

This figure "illustration.png" is available in "png" format from:

<http://arxiv.org/ps/cond-mat/0508100v5>

This figure "phase_diagram.png" is available in "png" format from:

<http://arxiv.org/ps/cond-mat/0508100v5>

This figure "pic_cleave2.jpg" is available in "jpg" format from:

<http://arxiv.org/ps/cond-mat/0508100v5>

This figure "reverse.png" is available in "png" format from:

<http://arxiv.org/ps/cond-mat/0508100v5>

This figure "simple_illustration.png" is available in "png" format from:

<http://arxiv.org/ps/cond-mat/0508100v5>

This figure "spm_J_7.jpg" is available in "jpg" format from:

<http://arxiv.org/ps/cond-mat/0508100v5>

This figure "spm_J_8.jpg" is available in "jpg" format from:

<http://arxiv.org/ps/cond-mat/0508100v5>

This figure "spm_J_65.jpg" is available in "jpg" format from:

<http://arxiv.org/ps/cond-mat/0508100v5>